PHILOSOPHICAL TRANSACTIONS OF THE ROYAL SOCIETY A MATHEMATICAL, PHYSICAL & ENGINEERING SCIENCES

Resonant Tunnelling Light-Emitting Diodes

C. Van Hoof, J. Genoe and G. Borghs

Phil. Trans. R. Soc. Lond. A 1996 **354**, 2447-2462
doi: 10.1098/rsta.1996.0111

Resonant tunnelling light-emitting diodes

By C. Van Hoof, J. Genoe and G. Borghs
Imec, Kapeldreef 75, B-3001 Leuven, Belgium

Resonant tunnelling light-emitting diodes (RTLEDs) are p–i–n diodes containing a double-barrier (or multi-barrier) resonant tunnelling structure in the intrinsic region of the diode. The simultaneous intraband tunnelling of electrons and heavy holes gives rise to injection electroluminescence from the quantum well and from the two accumulation layers on either side of the resonant tunnelling structure. The fast transient phenomena in these structures give rise to a fast response of the optical output otherwise only found in semiconductor lasers. Important aspects of the bipolar diode like speed and charge dynamics will be discussed.

1. Introduction

Optical properties of resonant tunnelling structures have been studied to obtain a clear understanding of the physics of tunnelling in general. The optical transient behaviour also makes them interesting candidates for applications where medium switching speed in the low GHz range is sufficient.

Electro-optical conversion in resonant tunnelling structures is applied in both ways. For instance light can influence the electrical behaviour of the device. Van Hoof (1992*a*) fabricated resonant tunnelling diodes acting as an optical modulator and detector and Higgins (1992) demonstrated the optical frequency tuning and modulation of a resonant tunnelling diode with laser light.

A bipolar resonant tunnelling diode also behaves like a fast light emitting diode. A variety of structures has been described in the literature, including light emitting diode structures and lasers as demonstrated amongst others by Van Hoof (1992*b*) and Sun (1993), respectively.

2. Light emission from resonant tunnelling structures

(*a*) *Electro-photoluminescence*

(i) *Steady-state luminescence*

Photoluminescence (PL) spectroscopy of resonant tunnelling diodes is really electro-photoluminescence and as such it contrasts with the PL at zero bias which received a lot of attention in the literature and is not described here. Contrary to the zero bias case, where the excitons are formed by e–h production within the well, the electron contribution to the exciton formation in the well originates from the time-independent stream of tunnelling electrons, and the hole contribution from photocreated holes. The large majority of holes are created outside the well and in a biased device are transported via drift-diffusion, tunnelling and thermionic emission through the structure.

Phil. Trans. R. Soc. Lond. A (1996) **354**, 2447–2462
Printed in Great Britain

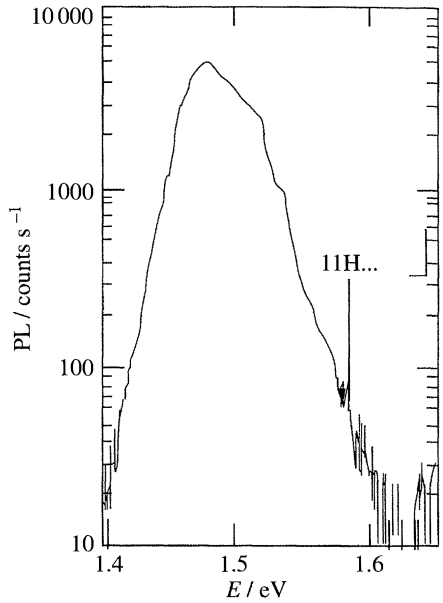

Figure 1. A typical example of a photoluminescence spectrum in the absence of external bias.

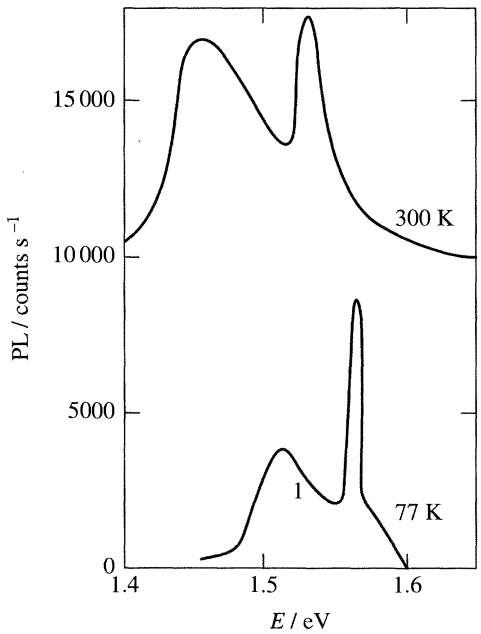

Figure 2. A spectrum for an at-resonance-biased tunnelling device. The quantum-well exciton at 1.582 eV is larger than the peak intensity of the GaAs luminescence. The top curve is taken at room temperature, the bottom curve at 77 K.

The quantum well luminescence increases by two orders of magnitude between zero bias and a bias V_p at resonance because of the huge increase in charge density at the peak voltage. As a result of fast diffusion, the photocreated holes reach the barriers of the RTS in a time $t < 300$ ps as estimated from experimental diffusion coefficients and minority carrier mobility. This is much less than the radiative recombination times

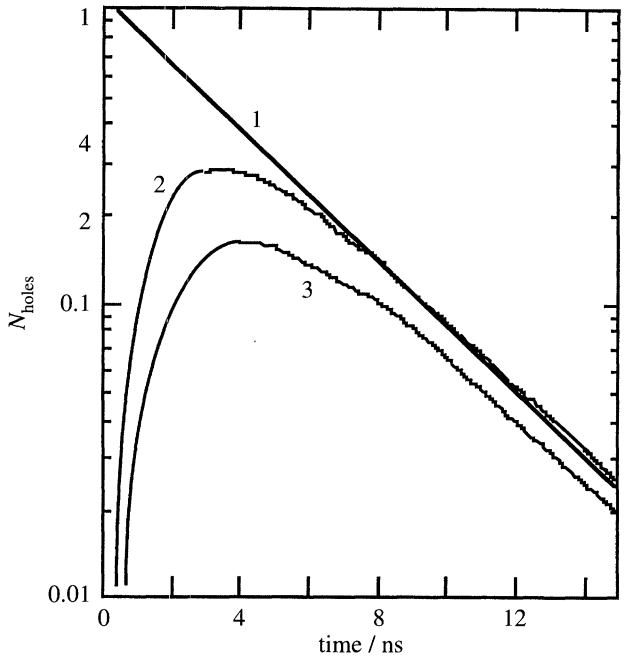

Figure 3. Calculated concentrations N1 in the accumulation layer, N2 in the quantum well and N3 in the emitter layer as a function of time.

in the n-type contact layers and a substantial hole accumulation occurs near the barrier. Even shorter timescales of the order of $t \leqslant 1$ ps are appropriate for the hole relaxation to the lowest level inside the quantum well via optical phonon emission as shown by Tatham (1989) and Fereira (1989). Hole inversion is impossible and even when the device is biased in resonance with a higher hole level the luminescent signal stems from the first heavy hole level (HH1) where the subbands are spaced by less than an optical phonon energy, non-radiative relaxation is dominated by acoustic phonon emission with much longer decay times $t \approx 200$ ps.

A typical example of a PL spectrum with and without bias for an n–i–n structure is shown (figures 1 and 2). In the absence of external bias (figure 1), quantum well luminescence is hardly observed at all, since it is dwarfed by the tail of the broad n^+GaAs luminescence. For increasing bias the quantum-well exciton PL at 1.582 eV is larger than the peak intensity of the GaAs luminescence (see figure 2). The top curve is taken at room temperature and shows a very strong exciton PL intensity, comparable to that of the GaAs layers, which is exceptional at room temperature.

(ii) *Transient transport phenomena*

Transient phenomena of transport and accumulation are investigated by time-resolved spectroscopy and also by steady-state measurements.

The time to traverse a barrier depends exponentially on the thickness and a change in barrier thickness from 1 to 4 nm alters time scales by three orders of magnitude. Optical time measurements with picosecond resolution are obtained using a streak camera, pulse probe techniques or degenerate four-wave mixing. Transients of accumulation is an important and well documented subject. A typical example of, for example, the charging and discharging of different hole reservoirs in a 4 nm barrier double-barrier resonant tunnelling structure is shown in figure 3.

Decay curves are measured at successive bias values and the population transients (figure 3) of the reservoirs are determined. They are governed by rate equations from which one can derive approximate time constants.

Young (1988) derived transient phenomena in a simple but indirect way from steady-state photoluminescence measurements and IV characteristics. In order for the current to be constant, the discharge or tunnelling escape has to be exactly compensated. As a consequence, one can write the current I as the transported charge Q divided by the tunnelling time t:

$$I = \frac{Q}{\tau} \Rightarrow \tau = \frac{Q}{I},$$

and this time constant is identical to the RC time constant, since for a discharging capacitor $RC = \mathrm{d}Q/\mathrm{d}I = Q/I$.

Intersubband scattering rates on the other hand have been determined by Faist (1993) by excited state differential absorption spectroscopy. Electrons are optically excited from the ground state to the first excited state of a doped quantum well. From measurements of the absorption cross section between excited states, a lifetime of 0.65 ps was deduced for a 8.5 nm GaAs quantum well and 0.8 ps for a 10 nm InGaAs quantum well. Moreover, from a lineshape analysis they derived an electron dephasing time of 0.26 ps which is much shorter than the period of coherent oscillation between coupled wells.

(iii) *Stark shift*

The quantum confined Stark effect (QCSE) allows us to determine the electric field over the structure by measuring the shift of the optical resonance frequency. It is a very powerful technique for determining charge redistributions and field partitioning over a heterostructure.

In the approximation of infinitely high barriers the energy shift of the ground state ΔE_1 is determined by a variational calculation given by Bastard (1983), which does not differ from a second-order perturbation approach, and is given by the following expression:

$$\Delta E_1 = -C_{\mathrm{var}} \frac{m^* e^2 E^2 L^4}{h^2},$$

with

$$C_{\mathrm{var}} = \frac{1}{8}\left(\frac{1}{3} - \frac{2}{\pi^2}\right)^2,$$

where E is the electric field and L the width of the quantum well.

A linear dependence on carrier mass indicates that the Stark shift of the heavy holes is much larger than that of the electrons by the ratio of the effective masses, i.e. a factor of 6.8 larger in GaAs. Larger quantum wells exhibit a larger Stark shift.

The effect of the electrical field on both the transmission probability and the interband transition energy of an RTS can be obtained by solving the Schrödinger equation for a double-barrier structure with linearly varying band edges (figure 4). Lippens (1989) showed that a plane wave approach introduces little error with respect to the Airy-function solution of the Schrödinger equation.

An experimental result (figure 5) shows an increase in the shift at tunnelling resonance, seen as a small bump at 0.25 V. This is attributed to bandgap renormalization due to the high density of charges in the well at this bias voltage. A narrowing of the

PHILOSOPHICAL TRANSACTIONS OF THE ROYAL SOCIETY A MATHEMATICAL, PHYSICAL & ENGINEERING SCIENCES

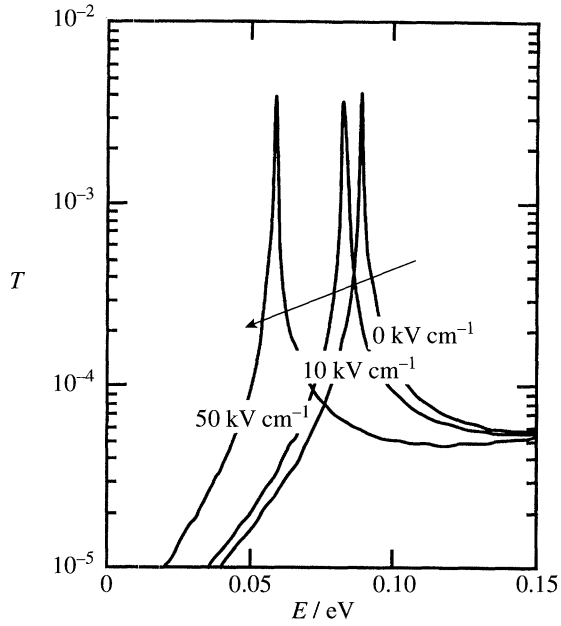

Figure 4. Calculated transmission probability and interband transition energy of a resonant tunnelling structure as a function of the electric field.

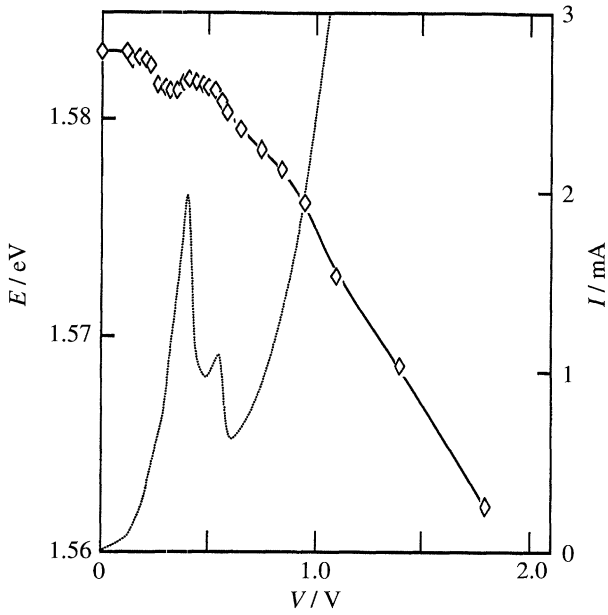

Figure 5. Experimentally determined shift in the tunnelling resonance as a function of electric field. The increase in the shift at tunnelling resonance, seen as a small bump at 0.25 V, is attributed to bandgap renormalization due to the high density of charges in the well at this bias voltage.

bandgap is a many-body effect determined by exchange interaction and correlation effects between the charges in the well.

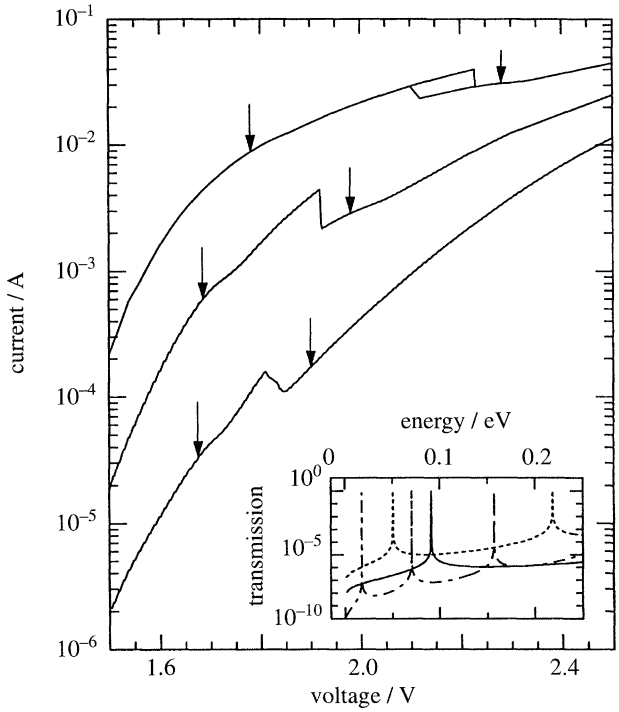

Figure 6. Current–voltage curves at 85 K of three different resonant tunnelling light emitting devices beyond flat band. The presence of small light hole resonances (arrows) and the larger due to electron resonant tunnelling is clear. Insert shows the transmission probabilities for electrons (solid curves) heavy holes (dashed curves) and light holes (dot-dashed).

(*b*) *Electroluminescence*

(i) *Current voltage characteristics of a bipolar resonant tunnelling light emitting device*

At 85 K the interesting part of the I–V curve of three different resonant tunnelling light emitting devices beyond the flat band is shown in figure 6 for comparison. The presence of small light hole resonances (arrows) and the larger resonances due to electron resonant tunnelling is clear. The relative positions are compatible with the energy-level calculations shown in figure 7. Heavy-hole resonances are not observed at 85 K. With decreasing barrier thickness from 5 nm (B5) to 4 nm (B4) to 3 nm (B3) (well width 5 nm) the currents through the device increase exponentially, which in turn increases the resonance voltage because of the increasing voltage drop across the contact resistance. Subtracting this voltage drop by assuming a series resistance of 10 Ω makes the corresponding light-hole and electron resonances of the three samples coincide. The series resistance is responsible for the observed current hysteresis in B3. The current through a resonant tunnelling structure consists of electrons, light-holes and heavy holes with a relative contribution of $0.3 : 1 : 5 \times 10^{-2}$. The overall peak-to-valley ratio of all resonances in these bipolar structures is smaller than in the corresponding unipolar n- or p-type structures because of the double component of the two non-resonant currents (electrons and holes). Because of the lower valence band barrier, the thermionic light-hole current and the non-resonant light-hole current (insert of figure 6) are even larger than the corresponding electron currents.

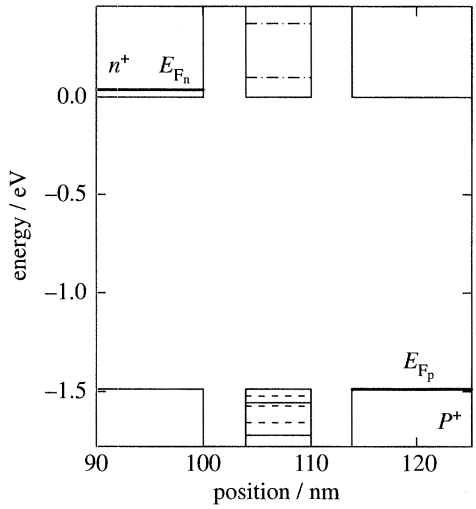

Figure 7. GaAs–AlGaAs band edges and calculated positions of different energy levels for electrons (E), light holes (LH) and heavy holes (HH) for a 4 nm barrier and 6 nm quantum well biased at 1.5 V. Pseudo-Fermi levels in the n and p regions are shown as bold curves.

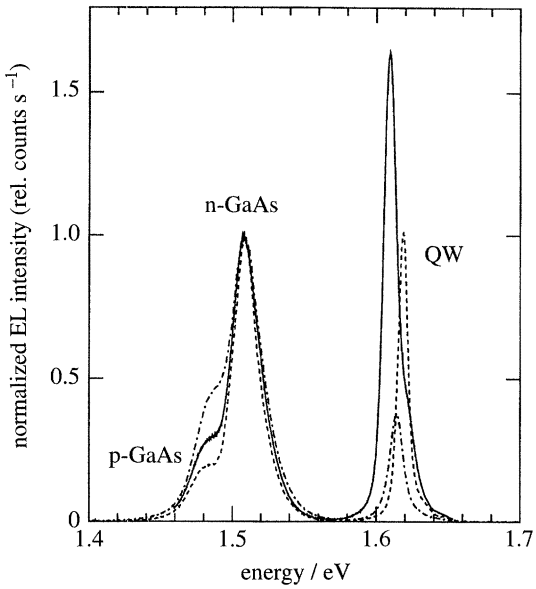

Figure 8. Normalized electroluminescence spectra for three samples (solid curve for B5, dashed for B4 and dot-dashed for B3). Emission from the n-GaAs (at 1.507 eV) and p-GaAs (at 1.485 eV) contact regions that can be distinguished spectrally.

(ii) *Spectra*

The normalized electroluminescence spectra beyond the onset of the bottom light-hole resonance are shown in figure 8 for the three samples (solid curve for B5, dashed for B4 and dot-dashed for B3). Beyond 1.5 V an electron and hole tunnelling current flows giving rise to emission from the n-GaAs (at 1.507 eV) and p-GaAs (at 1.485 eV) contact regions that can be distinguished spectrally because the combined effects of bandfilling and bandgap narrowing are opposite for n-doped and p-doped GaAs (Borghs 1989). Most of the emission from these two regions stems from the

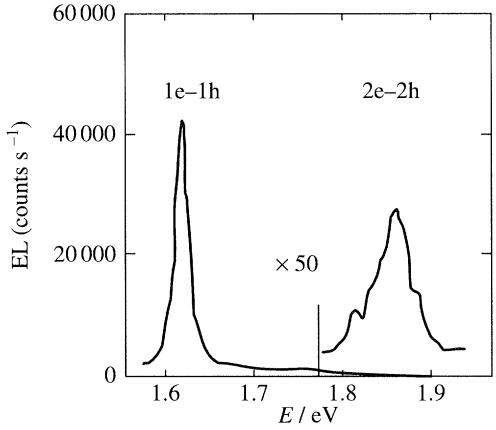

Figure 9. 77 K electroluminescence spectra as a function of photon energy of a resonant tunnelling light emitting diode showing visible light emission.

accumulation layers very close to the resonant tunnelling structure since the charge density is highest.

Even though the hole current consists mainly of light holes entering the resonant tunnelling structure, fast intersubband relaxation to the bottom heavy-hole subband will occur and the main quantum-well electroluminescence feature will be the electron to heavy-hole transition (at *ca.* 1.613 eV) and a smaller feature arises from electron to light-hole transitions (at *ca.* 1.647 eV). Because the tunnelling escape time decreases with decreasing barrier thickness, the relative quantum-well versus GaAs emission decreases from 1.7 to 1.0 or 0.35 respectively. These values do not translate linearly into tunnelling escape time ratios because the radiative recombination rate is a complex function of electron and light- and heavy-hole tunnelling times.

(iii) *Emission efficiency*

The total power emitted consists of the narrow quantum-well emission which adds up with the non-negligible contact-layer emission. With decreasing barrier width the optical power output exponentially increases and follows the overall slope of the $I(V)$. The optical power output at the electron resonance for B5 (B4, B3) is 1.10 μW (22.1 μW, 153.0 μW) and off-resonance 1.15 μW (28.8 μW, 233.0 μW). Dividing the emitted power by the consumed electrical power yields the quantum efficiency of about 0.6% at resonance. Local maxima are obtained at the hole resonances and the quantum efficiency steps at the electron resonance. This seemingly illogical step is obtained because the optical output relies on complicated charge redistribution and electron feedback as explained in § 3 *c*.

(*c*) *Occupation of higher subbands*

The EL spectra as a function of photon energy of a resonant tunnelling light emitting diode with 3 nm barriers and 5 nm well width is shown in figure 9. The EL at 1.61 eV is the emission from the lowest subbands in the RTS, the emission at 1.87 eV is EL from the second electron subband to the first heavy-hole subband. The relative intensity of the two transitions can be as as high as 1 : 30. The integrated spectral intensity of the 1.87 eV emission was 0.5% of the total spectrally integrated emis-

sion. With increasing temperature, the intensity of the visible emission decreases but persists to more than 150 K.

Due to fast LO phonon emission, the intersubband relaxation time is very short, and any occupation of higher subbands can hardly be achieved. At first, indeed only higher subband transitions were observed where the subband spacing was lower than the optical phonon energy. Acoustical phonon relaxation is two orders of magnitude slower. Non-thermal occupation of higher subbands was observed in semiconductor superlattices by Grahn (1990) via sequential resonant tunnelling resulting in photoluminescence from an excited electron subband to the lowest hole subband. Also, PL from higher subbands was observed under high carrier excitation conditions (at least in the kW cm^{-2} power density range). A population inversion between the 5th and 4th subband was also measured by Buckle (1994). They determined the occupation n_i of higher subbands by two time constants: the intersubband relaxation time τ_i and the tunnelling-out time τ_1 from E_1 (the first subband)

$$\frac{n_2}{n_1} = \frac{\tau_i}{\tau_1}.$$

3. Speed considerations

The switching speed of the resonant tunnelling light emitting diode is complicated by dynamics of charge redistribution in the different accumulation layers. In a first and simple approach switching times are only determined by tunnelling through the structure. The time a particle needs to traverse a barrier in double-barrier structures and multiple quantum wells has been the subject of numerous experimental studies.

(*a*) *Coherent tunnelling*

In the ideal case of no collisions and no relaxation, a wavepacket oscillates between two quantum wells with a well-defined Rabi frequency determined by the coupling between the two wells. The coupling strength itself is determined by the overlap of the wavefunctions in the two wells and as such is a function of the barrier parameters. Due to the coupling between the two levels an anticrossing occurs with an energy splitting determined by the strength of the coupling. The two levels are described by a symmetric and antisymmetric wavefunction as explained in elementary textbooks on quantum physics. The energy splitting at anticrossing determines the Rabi frequency at which a particle can oscillate between the two wells when it is excited as a coherent superposition of the symmetric and antisymmetric wavefunctions.

In a resonant tunnelling structure, the accumulation layer forms a two-dimensional well and the tunnelling from the contact layers into the quantum well of the structure can be described in the same way as coupling between two well-defined asymmetric quantum wells. In absence of scattering, the oscillation period T can be estimated following Luryi (1988*a*),

$$T = \frac{2\pi}{\omega} = \frac{\lambda L m_\mathrm{e}}{\hbar} \mathrm{e}^{2\pi L/\lambda},$$

where $\lambda = h/\sqrt{2m_\mathrm{e}(\phi - E_0)}$ is the de Broglie wavelength of the tunnelling particle, ϕ is the heterojunction barrier height.

By exciting the wide well when aligned with the narrow well, the oscillation and consequently the splitting could be directly measured by Leo (1991) using degenerate four-wave mixing and pulse probe techniques.

(b) Sequential tunnelling

The very short tunnelling times derived from the ideal case are hard to see in the experiments and most of the measured tunnelling times are in agreement with a relaxation time determined from a non-coherent tunnelling process, the sequential tunnelling times that can be derived from RC calculations. The deviation of the ideal situation is caused by the very short dephasing time which damps coherent oscillations between the two wells in a time much shorter than the oscillation period. According to Leo (1990) the tunnelling times are drastically increased by phase breaking collisions and relaxation processes. Because of the completely sequential behaviour of resonant tunnelling, time scales are determined by single-barrier tunnelling times. The single-barrier tunnelling time can be calculated from the intrinsic resistance capacitance (RC) product of a single barrier (Luryi 1985). The barrier resistance follows from the expression of the current density where the WKB approximation is used for the transmission probability for electrons through a single barrier. This yields

$$J(V) = \frac{e}{4\pi^2\hbar d^2} V_0(V) \exp\left[\frac{-2d}{\hbar}\sqrt{2m^* V_0(V)}\right],$$

where $V_0(V)$ is the bias-dependent barrier height. If we assume the barrier height to vary linearly with bias, and approximate the trapezoidal barrier by a square barrier (the plane-wave approach) then $\mathrm{d}V_0(V)/\mathrm{d}V \approx \frac{1}{2}$. By further neglecting the bias dependence of the pre-exponential factor, the tunnel resistance per unit area becomes

$$R \equiv \left(\frac{\mathrm{d}J}{\mathrm{d}V}\right)^{-1} = \left(\frac{4\pi\hbar d\lambda}{e^2}\right) \exp\left(\frac{4\pi d}{\lambda}\right),$$

with

$$\lambda(V) \equiv \frac{2\pi\hbar}{\sqrt{2m^* V_0(V)}},$$

where λ is the de Broglie wavelength of an electron tunnelling through the barrier. The capacitance of the barrier per unit area is given by $C' = \varepsilon/d$, and thus we find

$$\tau \equiv RC = \varepsilon \left(\frac{\hbar c}{e^2}\right)\left(\frac{\lambda}{c^2}\right) \exp\left(\frac{4\pi d}{\lambda}\right),$$

where c is the speed of light in vacuum. For a 3 nm AlAs barrier, $\varepsilon = 8.82\varepsilon_0, m^* = 0.12m_0$ and $V_0(V=0) = 1.06$ eV, we find a zero-bias tunnelling time of 400 ps.

The bias dependence of the tunnelling time is contained in the variation of τ with barrier height V_0 and hence with the applied voltage V. The single-barrier tunnelling time is exponentially dependent on barrier thickness (figure 10) and decreases exponentially with applied bias across the barrier (figure 11). In order to translate this bias into externally applied bias, depletion and accumulation have to be incorporated.

(c) Charge redistribution in resonant tunnelling light emitting diodes

(i) Spectra

As the external bias sweeps across a region of resonant tunnelling, either by electrons or by holes, the current shows a resonance and intuitively a similar behaviour in light output intensity is expected. This, however, is not necessarily the case, because of high charge densities in the quantum well at resonance. This manifests itself in two different ways: (i) the injection of electrons and holes is not mutually independent

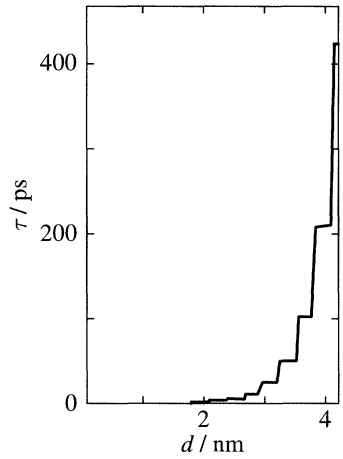

Figure 10. Calculated single-barrier *RC* time constant versus barrier thickness.

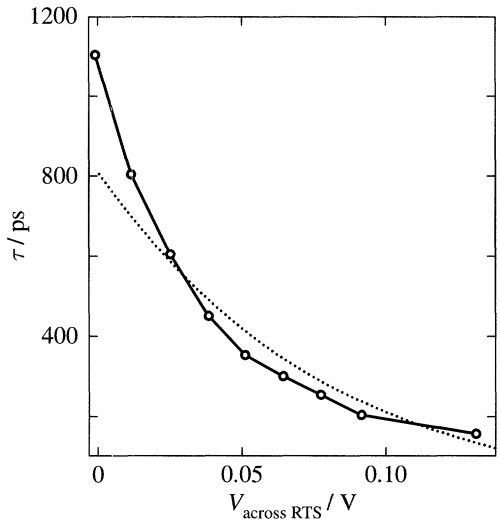

Figure 11. Tunnelling through a single barrier as a function of applied voltage. (—) Single barrier RC time constant as a function of voltage (–o–) experimental decay time constant for a 5 nm thick barrier.

and (ii) large differences between electrons and holes will lead to a light output that is governed by the number of minority carriers in the structure. A good illustration of this behaviour is given in figure 12 where an increase in light emission is observed (dashed curve) while the total current through the device is decreased three times (full curve).

The systematics of bipolar charge redistribution in double-barrier structures was investigated in detail with samples already described in § 2 *c*. As shown in figure 13 at a bias voltage near the electron resonance, the p-GaAs emission is large with respect to the n-GaAs emission especially for B5 and B4. This reflects a large electron current. The light emission at the n-doped contact layer in contrast is small since the hole injection is not resonantly enhanced and a large number of holes is lost to the quantum well for recombination. When the bias voltage is tuned off-resonance, the n-GaAs emission doubles (for B5 and B4) or triples (for B3) and the p-GaAs

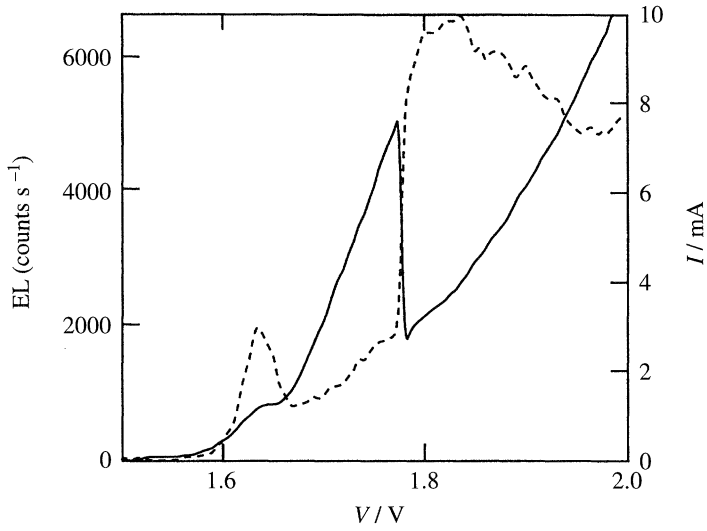

Figure 12. Light emission (dashed curve) versus total current (solid curve) as a function of bias voltage.

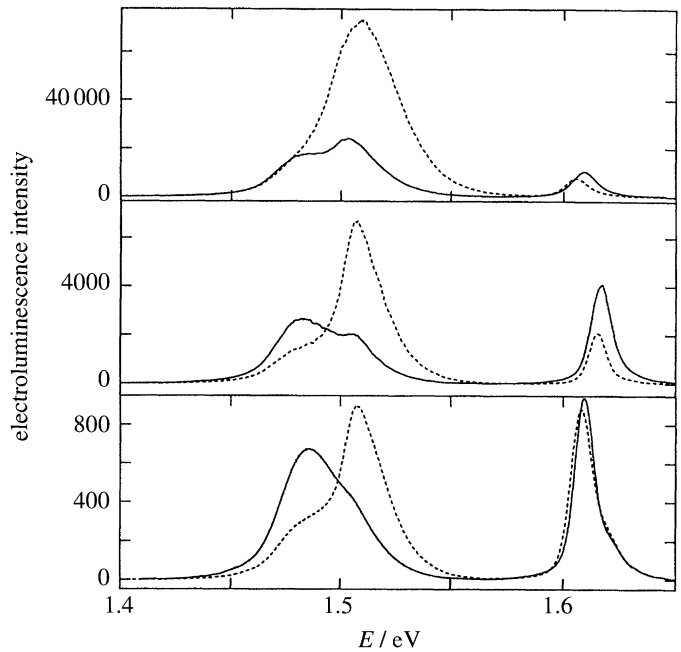

Figure 13. Electroluminescent spectra as a function of energy for a bias voltage at the electron resonance (solid curve) and off-resonance (dashed curve) for three structures B3, B4 and B5 (3, 4 and 5 nm barriers, 6 nm wells) from top to bottom, respectively. Electroluminescence peaks from the contact GaAs layers are at 1.47 eV (p-type) 1.51 eV (n-type) and 1.65 (QW luminescence).

emission is more than halved. The QW emission always decreases off-resonance and this decrease is 0.9 (B5), 0.5 (B4) and 0.7 (B3). The overall effect can be an increase of light emission when changing from on to off resonance as shown in figure 13 for a sample similar to B3. The increased radiative recombination at the n side is due to

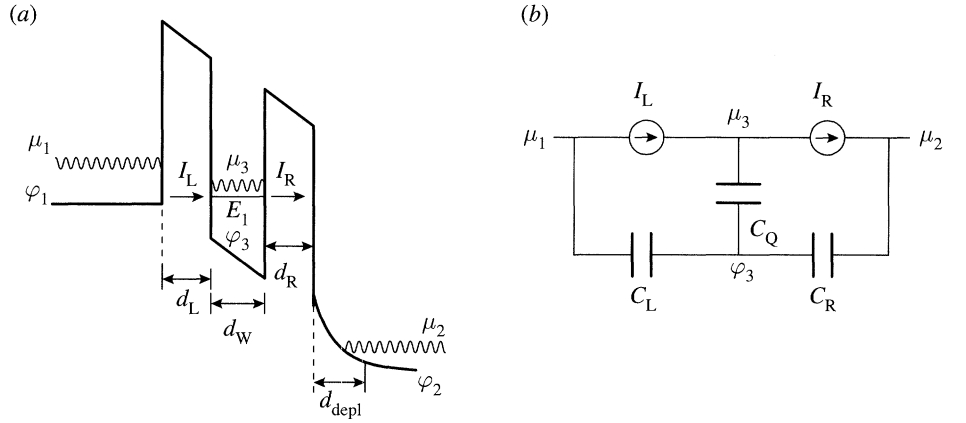

Figure 14. (*a*) Band diagram showing the relevant dimensions for the different capacitances used in the equivalent scheme. (*b*) Electrical equivalent circuit of the n–i–n resonant tunnelling structure including the so-called quantum capacitance C_q.

an increase of both carriers. The electron occupation increases to conserve external band-bending to compensate for the absence of electrons in the quantum well. This charge feedback pulls the n-GaAs accumulation layer concentration up. The increased hole injection comes from an increased band-bending across the quantum well and the barrier near the hole accumulation layer bringing the structure close to the second hole resonance. The decrease (for QW and p-GaAs) reflects the loss of electrons in the quantum well off-resonance and the decrease in the total electron current. The electron charge feedback influences strongly the capacitance of the double-barrier structure giving rise to a capacitance peak as explained below.

(ii) *Dynamics of charge redistribution*

To determine the timescales of this charge feedback and the optical switching involved with it we need a more complete approach to the double-barrier structure. A detailed study of transients taking charge redistribution into account (for a homotype resonant tunnelling structure) has been published by Genoe (1991) and we refer to this study for further reading. In this paper the charging of the quantum well was described as a quantum capacitance C_q defined according to an idea first formulated by Luryi (1988*b*):

$$C_q = \frac{\delta Q_w}{\delta V_q} = -e\frac{\delta Q_w}{\delta \mu_3},$$

with

$$-eV_q = \mu_3 - \phi_3,$$

where ϕ_3 is the conduction band edge in the middle of the well.

By considering an equivalent circuit consisting of the elements given schematically in figure 14*b* including the so-called quantum capacitance C_q, a general formula for capacitance and conductance as a function of voltage was determined. The tunnelling through the well is taken to be completely sequential with a localized quantum well electron obeying Fermi–Dirac statistics. From the calculations, the charge feedback is immediately clear. A capacitance increase when charging the well was predicted by others using a constant capacitance. Now a much larger increase in the capacitance when switching from on- to off-resonance was also explained for the first time with

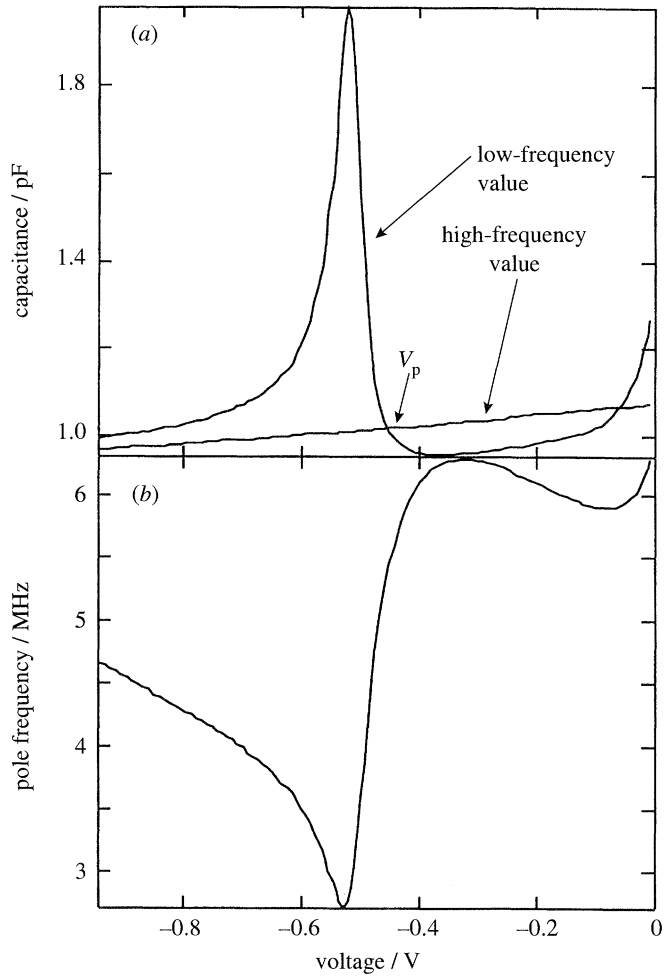

Figure 15. Value of the capacitance in the high- and low-frequency regime. In the low-frequency regime a capacitance peak is expected which is confirmed by experimental measurements. In the high frequency oscillation regime, the capacitance peak disappears. The pole frequency marks the boundary between high- and low-frequency behaviour.

this theory. The capacitance peak is indirectly confirmed by the optical measurements explained above. The value of the capacitance in the high- and low-frequency regime is shown in figure 15. In the low-frequency regime a capacitance peak is expected which is confirmed by experimental measurements. In the high-frequency oscillation regime, the capacitance peak disappears.

The pole frequency marks the boundary between high- and low-frequency behaviour. In the high-frequency regime, the system is not able to relax fast enough to an equilibrium Fermi–Dirac state and the capacitance peak disappears as well as the optical modulations related to this capacitance peak.

The pole frequency determines the timescales and thus the optical switching speed of the resonant tunnelling light emitting diode. In figure 16 we show the pole frequency of the structures as a function of the barrier thickness for a n–i–n structure. The pole frequency changes drastically with barrier thickness as can be expected from a tunnelling process.

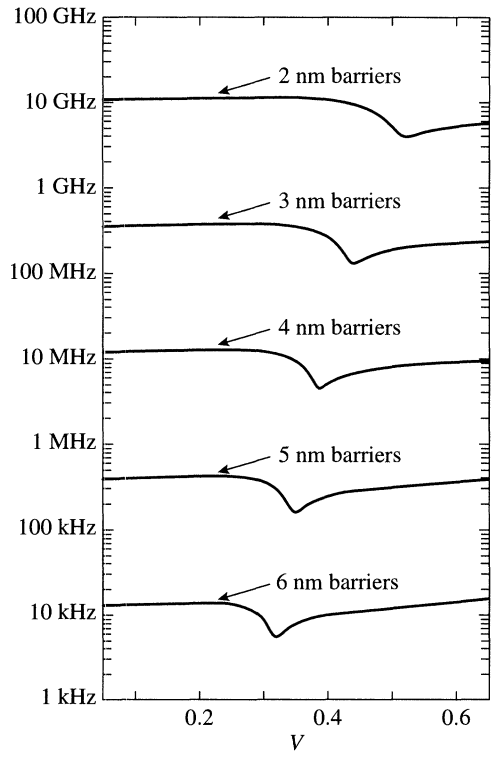

Figure 16. Pole frequency of the structures as a function of the barrier thickness for an n–i–n structure.

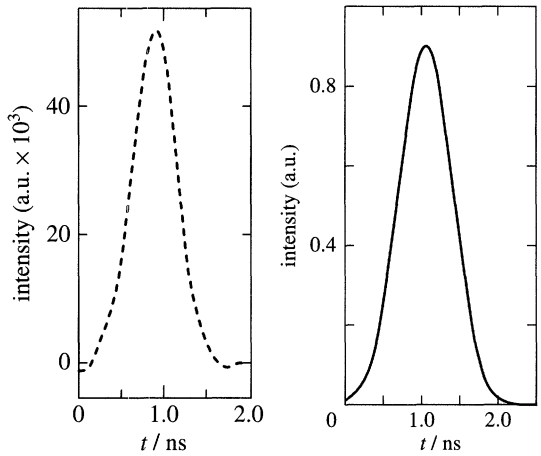

Figure 17. Large-signal modulation of the room-temperature optical output of the RTLED, before deconvolution (right) and after deconvolution (left) with the instrumental response of the photodetector. The large-signal bandwidth is larger than 700 MHz. Small-signal modulation bandwidth is at least 2 GHz.

(*d*) *Room-temperature high-speed RTLEDs*

Conventional (i.e. double-heterostructure) AlGaAs–GaAs LEDs can follow large-signal modulation to low MHz. The inherent limitation is the radiative recombination time. Indeed, both switch-on and switch-off are governed by the radiative recombi-

nation lifetime. As a consequence conventional LEDs are limited to approximately a few hundreds of MHz. Ultra high-doping of the active layer of conventional LEDs can increase the speed by reducing the radiative lifetime. But at the same time, the increased Auger recombination will reduce the quantum efficiency to very low levels. Resonant tunnelling light emitting diodes can be driven at room temperature with a large signal modulation (0 V to 3 V, risetime and fall time each 250 ps, total electrical pulse width 1.5 ns—equipment limited). The optical output measured with an avalanche photodiode and a 2 GHz digitizing oscilloscope is shown in figure 17. Without deconvolution of the instrumental response, the 10–90% risetime and fall time of the optical outputs were 500 ps. After deconvolution (second figure) 10–90% rise and fall times were 300 ps.

As a consequence the large-signal bandwidth is larger than 700 MHz and the 3 dB bandwidth (where the optical response is halved) is larger than 1.5 GHz.

References

Bastard, G., Mendez, E. E., Chang, L. L. & Esaki, L. 1983 *Phys. Rev.* B **28**, 3241.

Borghs, G., Bhattacharya, K., Deneffe, K., Van Mieghem, P. & Mertens, R. 1989 *J. Appl. Phys.* **66**, 4381.

Buckle, P. D., Cockburn, J. W., Teissier, R. J., Willcox, A. R. K., Whittaker, D. M, Skolnick, M. S., Smith, G. W., Grey, R., Hill G. & Pate, M. A. 1994 *Semicond. Sci. Technol.* **9**, 533.

Faist, J., Capasso, F., .Sirtori, C., Sivco, D. L., Hutchinson, A. L., Chu, S. N. G. & Cho, A. 1993 *Appl. Phys. Lett.* **63**, 1354.

Fereira, R. & Bastard, G. 1989 *Phys. Rev.* B **40**, 1074.

Genoe, J., Van Hoof, C., Van Roy, W., Smet, J. H., Fobelets, K., Mertens, R. P. & Borghs, G. 1991 *IEEE Trans. Electron. Devel.* **38**, 2006.

Grahn, H. T., Schneider, H., Rühle, W. W., von Klitzing, K. & Ploog, K. 1990 *Phys. Rev. Lett.* **64**, 2426.

Grahn, H. 1992 Habilatations thesis, Max-Planck-Institut für Festkörperforschung, Stuttgart.

Higgins, T. P. 1992 *Electron. Lett.* **28**, 1574.

Leo, K., Shah, J., Gordon, J. P., Damen, T. C., Miller, D. A. B., Tu, C. W. & Cunningham, J. E. 1990 *Phys. Rev.* B **42**, 7065.

Leo, K., Shah, J., Göbel, E. O., Damen, T. C., Schmitt-Rink, S., Schäfer, W. & Köhler, K. 1991 *Phys. Rev. Lett.* **66**, 201.

Lippens, D., De Saint Pol, L., Bouregba, R., Mounaix, P. & Vinchon, T. 1989 *Rev. Phys. Appl.* **24**, 17.

Luryi, S. 1985 *Appl. Phys. Lett.* **47**, 490.

Luryi, S. 1988*a* *Sol. Stat. Commun.* **65**, 787.

Luryi, S. 1988*b* *Appl. Phys. Lett.* **52**, 501.

Tatham, M. C., Ryan, J. F. & Foxon, C. T. 1989 *Phys. Rev. Lett.* **63**, 1637.

Sun, H. C., Davis, L., Sethi, S. J. Singh, J. & Bhattacharya, P. 1993 *Photon. Technol. Lett.* **5**, 870.

Van Hoof, C. 1992*a* Ph.D. thesis, Katholieke Universiteit, Leuven.

Van Hoof, C., Genoe, J., Mertens, R., Borghs, G. & Goovaerts, E. 1992*b* *Appl. Phys. Lett.* **60**, 77.

Young, J. F, Wood, B. M., Aers, G. C. Devine, R. L. S., Liu, H. C., Buchanan, M., SpringThorpe, A. J. & Mandeville, P. 1988 *Phys. Rev. Lett.* **20**, 2085.

PHILOSOPHICAL TRANSACTIONS OF THE ROYAL SOCIETY A MATHEMATICAL, PHYSICAL & ENGINEERING SCIENCES